ACS APPLIED ENERGY MATERIALS
Cite This: ACS Appl. Energy Mater. 2018, 1, 2275−2282
Article
www.acsaem.org

Direct Observation of the Impurity Gettering Layers in Polysilicon-Based Passivating Contacts for Silicon Solar Cells

AnYao Liu,*,† Di Yan,† Jennifer Wong-Leung,‡ Li Li,§ Sieu Pheng Phang,† Andres Cuevas,† and Daniel Macdonald†

†Research School of Engineering, College of Engineering and Computer Science,, Australian National University, Canberra, Australian Capital Territory 2601, Australia

‡Department of Electronic Materials Engineering, Research School of Physics and Engineering, Australian National University, Canberra, Australian Capital Territory 2601, Australia

§Australian National Fabrication Facility, Department of Electronic Materials Engineering, Research School of Physics and Engineering, Australian National University, Canberra, Australian Capital Territory 2601, Australia

Downloaded via COPYRIGHT CLEARANCE CTR DCMT DLVRY on April 15, 2024 at 11:48:57 (UTC).
See https://pubs.acs.org/sharingguidelines for options on how to legitimately share published articles.

ABSTRACT: The formation of certain types of doped polysilicon passivating contacts for silicon solar cells is recently reported to generate very strong impurity gettering effects, revealing an important additional benefit of this passivating contact structure. This work investigates the underlying gettering mechanisms by directly monitoring the impurity redistribution during the contact formation and subsequent processes, via a combination of secondary ion mass spectrometry (SIMS), transmission electron microscopy (TEM), and minority carrier lifetime techniques. Microscopic features of the phosphorus and boron diffusion-doped polysilicon passivating contacts are also presented. Iron is used as a marker impurity in silicon to enable direct quantification of its concentration change in the bulk of the silicon wafers and in the surface layers that compose the contact structure. The results conclusively show that, for phosphorus-doped polysilicon passivating contacts, impurities are relocated from the silicon wafer bulk to the heavily phosphorus-doped polysilicon layer; while for the boron diffusion-doped polysilicon, the boron-rich layer (a silicon−boron compound) accounts for the majority of the gettering action.

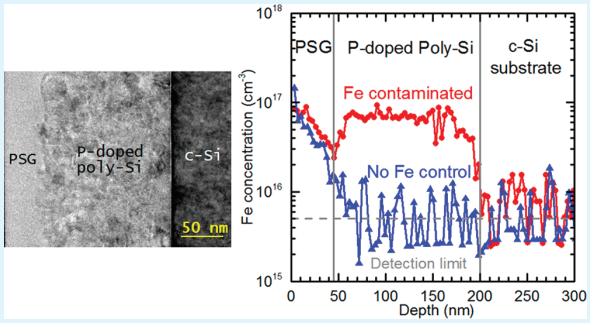

KEYWORDS: *gettering, polysilicon passivating contacts, silicon, iron, solar cells*

1. INTRODUCTION

Efficiency loss due to carrier recombination at the metal−silicon interface is a significant limitation in the conventional silicon solar cell designs. Passivating contacts overcome this limitation by providing both effective transport of majority carriers and excellent suppression of minority carrier recombination at the interface. As a result, passivating contacts have become an enabler in the recent cell efficiency gains,[1−3] breaking the long-standing efficiency record held by the passivated emitter rear locally diffused (PERL) silicon solar cells.[4]

A doped polycrystalline silicon (polysilicon, or poly-Si) film with a thin silicon oxide (SiO_x) interlayer is one of the most common and effective approaches to fabricating passivating contacts in silicon solar cells, as has been demonstrated in the reported record cell efficiencies.[2,3,5] Polysilicon based passivating contacts have been used in other silicon devices such as in bipolar junction transistors (BJT) to improve the device performance.[6,7] In addition to the efficiency gain, the polysilicon passivating contacts have high-temperature stability and a relatively simple fabrication process (no patterning required), making them particularly appealing to the silicon solar cell manufacturing industry.

Another significant efficiency loss channel in solar cells is carrier recombination via impurities and defects (especially impurity-decorated defects) in the silicon wafer bulk. Impurity gettering is therefore a vital aspect of the cell fabrication process, particularly for the mass-produced solar cells made from cheaper solar-grade silicon materials and in less well controlled contamination environments.

It is recently reported that certain types of polysilicon passivating contacts can achieve effective impurity gettering during contact formation, while maintaining their excellent passivating contact quality.[8,9] This demonstrates an added advantage of the polysilicon passivating contact, making it a complete solution to addressing the carrier transport, and surface and bulk recombination losses in silicon solar cells,

Received: March 8, 2018
Accepted: April 19, 2018
Published: April 19, 2018

© 2018 American Chemical Society

DOI: 10.1021/acsaem.8b00367
ACS Appl. Energy Mater. 2018, 1, 2275−2282

REC Exhibit 1028, Page 1 of 8

which further strengthens its potential for the mass production of high-efficiency solar cells.

This work aims to gain a better understanding of the impurity gettering effects of polysilicon passivating contacts. This would enable contacts with more effective gettering to be developed, and the reason behind the different gettering efficiencies from contacts fabricated with different techniques[8,9] could be explained and resolved. We use iron (Fe) as a marker impurity in silicon to qualitatively and quantitatively assess its redistribution during contact formation and subsequent processes, which allows a direct identification of the gettering sites in polysilicon passivating contacts. The Fe concentration in the bulk of the silicon wafers is measured by a carrier lifetime based technique,[10,11] and the Fe distribution and concentration in the surface polysilicon passivating contact layers and the near-surface regions of the silicon wafer bulk are measured by secondary ion mass spectrometry (SIMS). High-resolution transmission electron microscopy (HR-TEM) and scanning TEM (STEM) are applied to understand the surface layer structures and compositions, and to reveal microscopic features of the polysilicon passivating contacts. The polysilicon layers are ex-situ-doped via a conventional thermal diffusion using $POCl_3$ or BBr_3 sources, a process that is directly compatible with the existing cell fabrication tools in industry.

2. EXPERIMENTAL DETAILS

A flowchart of the experimental procedures is shown in Figure 1.

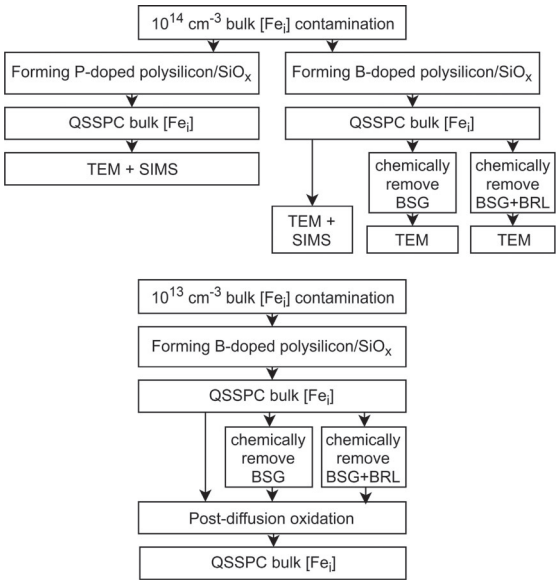

Figure 1. Flowchart of the experimental procedures.

This work used high-quality float-zone (FZ) silicon wafers with precise doses of intentional bulk Fe contamination. Fe is introduced into the Si wafer bulk via ion implantation and subsequent distribution annealing, as detailed in ref 8. The boron-doped p-type FZ-Si wafers had a resistivity of 0.9 Ω cm and a thickness of 180 ± 5 μm after saw damage etching. After Fe implantation and distribution annealing, the wafers were contaminated with either 10^{13} cm^{-3} or 10^{14} cm^{-3} bulk interstitial Fe concentrations ([Fe$_i$]).

The Fe-contaminated silicon wafers were then subjected to the formation of phosphorus or boron diffusion-doped polysilicon/oxide passivating contacts. Details of the fabrication technique can be found in refs 12 and 13. Symmetric polysilicon contact structures were fabricated on both sides of the wafers. The samples used for SIMS and TEM measurements had a high initial bulk [Fe$_i$] of 10^{14} cm^{-3}, in order to improve SIMS sensitivity to the Fe concentration in polysilicon. Thin silicon oxide layers were grown on the silicon wafer surfaces via immersion in a 68 wt % nitric acid bath at 90 °C for 30 min, resulting in an oxide thickness of around 1.3−1.4 nm, from previous ellipsometry measurements.[12] The samples were then coated with intrinsic amorphous silicon (a-Si) films from plasma-enhanced chemical vapor deposition (PECVD), at an on-sample temperature of ∼250 °C. The samples were held at ∼250 °C for a total of 1 h. Deposited dielectric films such as PECVD silicon nitride and atomic-layer-deposited (ALD) aluminum oxide have been reported to cause impurity gettering effects at elevated temperatures where the metals are sufficiently mobile.[14−16] It is presently unknown whether a-Si films possess similar gettering effects or not. Nevertheless, the moderate diffusivity of Fe$_i$ in silicon[17] at 250 °C limits any possible surface gettering effects to less than 20% during the PECVD deposition process, which is rather small compared to the amount of Fe$_i$ being gettered during the polysilicon passivating contact formation (>99.9%).[8] A typical a-Si film thickness, as was used in our previous studies,[8,12,13] is 30−40 nm. Much thicker films of 150−200 nm were deposited for the SIMS and TEM samples in this study, to enable clear layer distinction, and to avoid the impact of surface contamination and surface-related measurement artifacts when interpreting the SIMS depth profiles. The a-Si/oxide coated samples were then subjected to thermal diffusions in quartz tube furnaces in either $POCl_3$ or BBr_3 sources. $POCl_3$ diffusion was carried out at 890 °C for a total of 40 min, and BBr_3 diffusion was performed at 900 °C for 45 min. The samples were loaded in and out of the furnaces at 700 °C, with a ramp-up and ramp-down rate of 10 °C/min. The thermal diffusion processes also resulted in a partial recrystallization of the amorphous silicon into polycrystalline silicon, as will be revealed by TEM results.

The Fe$_i$ concentrations in the silicon wafer bulk were measured before and after the polysilicon contact formation. A WCT-120 tool from Sinton Instruments was used to measure the effective minority carrier lifetime curves.[18] From the carrier lifetimes measured before and after Fe−B pair dissociation via strong illumination, the bulk Fe$_i$ concentrations were determined.[10,11,19] The reported error bars in [Fe$_i$] came from assuming a 10% uncertainty in the measured lifetimes before and after Fe−B pair breaking.

SIMS depth profiling was used to measure the Fe and dopant (P or B) concentrations in the polysilicon passivating contacts and the near-surface silicon substrate. The measurements were conducted by EAG Laboratories. The nominal depth resolution was ∼2 nm/step, although the actual resolution was likely much larger as the bombarded ions tend to become intermixed during the depth profiling.

To assess the surface layer structure and chemical composition, high-resolution TEM (HR-TEM), and scanning TEM (STEM) coupled with energy dispersive X-ray spectroscopy (EDS) mapping and high-angle annular dark-field (HAADF) imaging, were employed to examine the cross-section of the near-surface regions, using a JEOL JEM-2100F TEM instrument. The TEM lamellae were prepared by focused ion beam (FIB), with an FEI Helios 600 NanoLab instrument. Gallium (Ga) ion beam was used in the FIB. Following similar low-energy FIB techniques,[20] relatively low-energy Ga beams (16 keV, 8 keV, and finally 2 keV) were sequentially used in this work to carefully polish the TEM lamellae to minimize Ga damages. No Ga-related artifacts were observed in the lamellae by TEM.

The samples for SIMS and TEM analyses had the phosphosilicate glass (PSG) or boron silicate glass (BSG) retained on the sample surfaces. In order to identify the location and thickness of the boron-rich layer (BRL)[21−23] in the boron diffusion-doped polysilicon, additional samples with different surface layers were prepared for TEM examinations. One sample had the BSG layer removed in dilute HF solution, in which case the remaining surface layers were BRL/polysilicon. The sample surfaces were found to remain hydrophilic in HF solution, which is a well known characteristic of the BRL,[21] confirming its presence at the surface layer after the BSG removal. The other sample had both the BSG and BRL layers removed, with the remaining layer being polysilicon alone. The BSG was removed in HF,

DOI: 10.1021/acsaem.8b00367
ACS Appl. Energy Mater. 2018, 1, 2275−2282

REC Exhibit 1028, Page 2 of 8

and the BRL was removed by boiling nitric acid and HF. By immersing the samples in boiling nitric acid, the surface BRL becomes oxidized into BSG and can thus be etched off in HF.[22,24] The two steps were repeated until the sample surfaces became hydrophobic, indicating the complete removal of the BRL, and revealing the polysilicon as the remaining surface layer. Oxidation of the polysilicon in boiling nitric acid is a self-limiting, very slow process.[25] Partial removal of the polysilicon layer in boiling nitric acid is limited to no more than a few nanometers.

In order to confirm the main gettering site in boron diffusion-doped polysilicon contacts, post-diffusion oxidation was carried out to examine the bulk [Fe_i] changes, as an oxidized BRL releases its gettered impurities back into the silicon bulk at moderate and high temperatures.[26] The boron-doped polysilicon samples from ref 8. were used for the oxidation experiment. These samples had a lower initial [Fe_i] of 10^{13} cm^{-3} to enable accurate lifetime-based bulk [Fe_i] measurements. After contact formation, the bulk Fe_i concentrations were found to drop to (0.4−1.5) × 10^{10} cm^{-3}.[8] Post-diffusion oxidation was performed on the samples with different remaining surface layers: BSG/BRL/polysilicon layers, BRL/polysilicon layers, and polysilicon layer alone. For the samples with either BSG/BRL/polysilicon or BRL/polysilicon layers, oxidation was conducted at 930 °C for 80 min in dry oxygen, with a 10 °C/min ramp-up and ramp-down to 700 °C. This condition is more than sufficient to fully oxidize the BRL.[23,26] Complete oxidation of the BRL was confirmed in our experiment, as the sample surfaces became hydrophobic in HF after the oxidation step. The sample with only the polysilicon layer remaining was oxidized at 930 °C for 4 h in dry oxygen to allow full oxidation of the 30−40 nm thick polysilicon layer. The bulk Fe_i concentrations were measured after oxidation.

3. RESULTS

3.1. Gettering in Phosphorus Diffusion-Doped Polysilicon Passivating Contact. The layer structure of the $POCl_3$ diffusion-doped polysilicon contact is shown in Figure 2. The different layers can be easily distinguished because of the very different crystal structures: PSG is amorphous, the P-doped poly-Si layer is partially crystallized (which confirms that the PECVD deposited a-Si films partially recrystallize into poly-Si during thermal diffusion in a dopant source), and the silicon wafer bulk is crystalline. The crystal phases were also confirmed by the respective electron diffraction patterns (not shown).

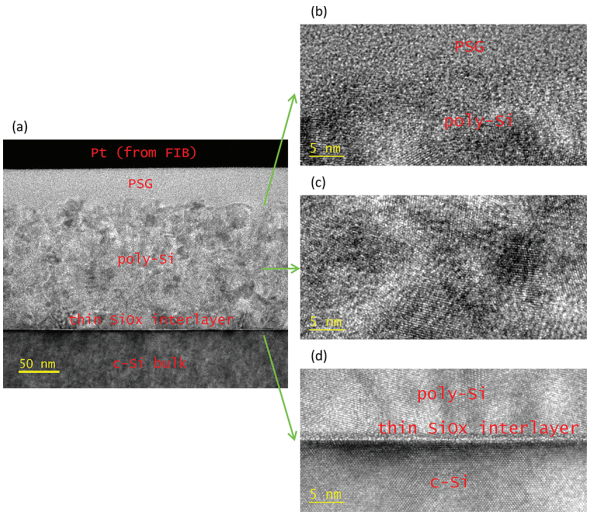

Figure 2. TEM and HR-TEM images of the $POCl_3$-diffused polysilicon contact: (a) structure overview; (b) PSG/poly-Si interface; (c) middle of the poly-Si layer; (d) poly-Si/thin SiO_x interlayer/c-Si interface.

Further evidence of the layer structure is demonstrated by the HAADF-STEM image and EDS-STEM maps and line scans shown in Figure 3. The 40−50 nm thick surface layer is revealed to be rich in oxygen and lean in silicon, which confirms its identification as the PSG (a mixture of P_2O_5 and SiO_2) layer. It is interesting to note that some PSG "fingers" extend into the poly-Si layer, which may relate to the porous structure and nonplanar surface of the low-temperature deposited a-Si films that result in uneven penetration of the PSG layer. The thin SiO_x interlayer, in between the doped poly-Si layer and the crystalline silicon (c-Si) wafer bulk, can also be clearly seen in Figure 3.

The sample shown in Figures 2 and 3 had a precise amount of dissolved Fe (i.e., Fe_i) introduced into the silicon wafer bulk prior to forming the phosphorus-diffused polysilicon surface contacts on both sides. After contact formation, the Fe_i concentration in the silicon wafer bulk dropped from 10^{14} cm^{-3} to 2 × 10^{10} cm^{-3}. Unfortunately, Fe could not be clearly detected by EDS-STEM mapping, because of its low concentration and moderate atomic mass. SIMS was therefore used to reveal the Fe concentration in the surface regions, as shown in Figure 4. The layer structure, as marked on the SIMS depth profiles in Figure 4, is from the TEM and STEM analyses in Figures 2 and 3.

As shown in Figure 4, the phosphorus-doped polysilicon layer contains a high concentration of Fe for the Fe-contaminated sample, whereas the Fe concentration in the no-Fe control sample remains at the detection limit. Note that the apparent [Fe] increase toward the sample surfaces in the top tens of nanometres, as observed on both Fe-contaminated and no-Fe samples, can be attributed to surface contamination and near-surface measurement artifacts. For the Fe-contaminated sample, the Fe concentration in the surface P-doped polysilicon layer, from SIMS measurements, amounts to a bulk Fe concentrtion of 9.5 × 10^{13} cm^{-3} for a 180-μm thick wafer with symmetric polysilicon structure on both sides. This agrees very well with the initial bulk Fe contamination of 10^{14} cm^{-3}, further proving that Fe is gettered from the silicon wafer bulk to the P-doped polysilicon surface layers during contact formation.

Heavy doping of the polysilicon layer by P atoms is confirmed by the SIMS [P] profile in Figure 4. It is interesting to note that the P concentration in the poly-Si layer is higher than the SIMS measured P concentrations in the c-Si surface regions for direct $POCl_3$ diffusion on c-Si wafers.[27−29] This may relate to the high density of grain boundaries in poly-Si, where dopant accumulation and precipitation take place.[30−32] The blocking effect of the interfacial SiO_x on the diffusion of P atoms, and the thinner poly-Si layers compared to the doped c-Si surface regions (tens to a couple hundred of nanometers of poly-Si as compared to several hundred nanometers to a few micrometers in c-Si), may also contribute to a higher level of dopant supersaturation in the poly-Si layer.

As the remaining Fe_i concentration in the silicon wafer bulk (2 × 10^{10} cm^{-3}) dropped to below the solubility limit of Fe_i in silicon at 700 °C (10^{11} − 6 × 10^{11} cm^{-3}),[17,33] which is the furnace unloading temperature, it is evident that the gettering effect of the P-doped polysilicon layer occurs via impurity segregation. As reported previously, an undoped polysilicon layer exhibits much weaker gettering effects, indicating the importance of heavy phosphorus doping on the gettering effectiveness.[8] Phosphorus diffusion gettering (PDG) has been

DOI: 10.1021/acsaem.8b00367
ACS Appl. Energy Mater. 2018, 1, 2275−2282

REC Exhibit 1028, Page 3 of 8

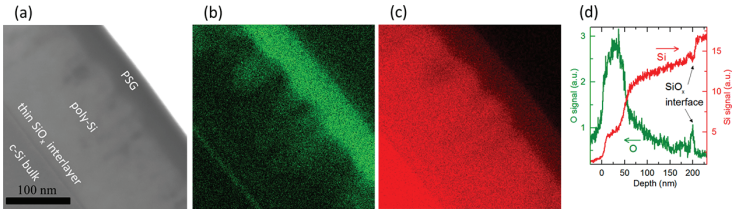

Figure 3. (a) HAADF-STEM image of the $POCl_3$-diffused polysilicon contact. (b, c) Corresponding EDS-STEM maps of oxygen (O K-map) and silicon (Si K-map), respectively. (d) Line scans across the EDS-STEM maps shown in panels b and c.

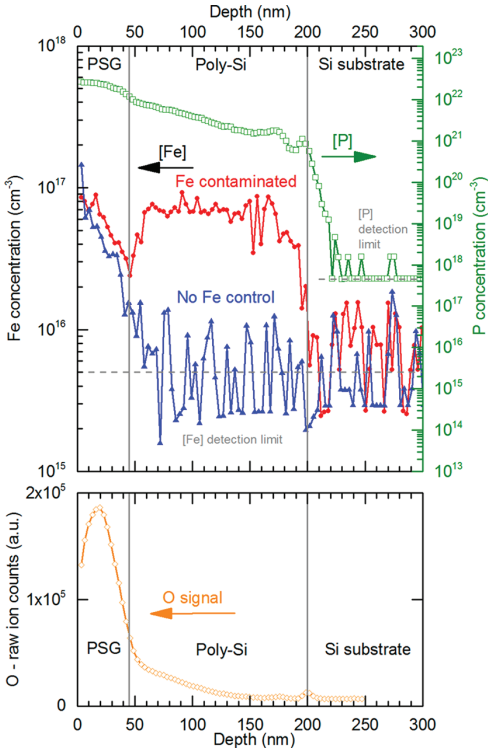

Figure 4. SIMS Fe and P concentrations (top) and uncalibrated O signal (bottom) in $POCl_3$-diffused polysilicon passivating contact layers and the near-surface silicon substrate, for samples with and without an initial bulk Fe contamination of 10^{14} cm^{-3} prior to the contact formation.

long known and applied in both microelectronics and photovoltaics, yet there are multiple explanations in the literature for the underlying physical mechanisms (see, e.g., refs29 and 34. and the references therein). A more recent model proposed by Schön et al. was shown to explain a range of experimental results reported in the literature concerning the PDG of Fe.[29] The dominant gettering mechanisms were attributed to the reactions of (a) Fe with oxygen complexes and (b) Fe with either electrically active or inactive P atoms.[29] As shown in Figure 4, the SIMS Fe profile demonstrates a plateau in Fe concentration in the P-doped polysilicon layer, whereas both the SIMS P concentration and the uncalibrated O signal (SIMS in Figure 4 and EDS-STEM in Figure 3d) show a varying profile. The total P concentration measured by SIMS is likely dominated by the electrically inactive P atoms, as the active P concentration in Si at equilibrium is only 3×10^{20} cm^{-3} at 890 °C,[35] much smaller than the total P concentration shown in Figure 4. A comparison of the Fe, P, and O profiles therefore suggests that the gettering of Fe in the P-doped polysilicon layer cannot be explained by a simple correlation with the presence of a single impurity species. Fe may also be gettered by the *heavily P-doped* grain boundaries and defects in the polysilicon layer (noting that the undoped polysilicon does not getter efficiently[8]). Other mechanisms may be at play as well. Further investigations are required to elucidate the exact gettering mechanisms on an atomic scale, and determine their relative contributions to the total effect.

3.2. Gettering in Boron Diffusion-Doped Polysilicon Passivating Contact. The layer structure of the BBr_3 diffusion-doped polysilicon contact has also been examined by TEM, HAADF-STEM, and EDS-STEM, as shown in Figures 5 and 6. Similar to the PSG (a mixture of P_2O_5 and SiO_2), the

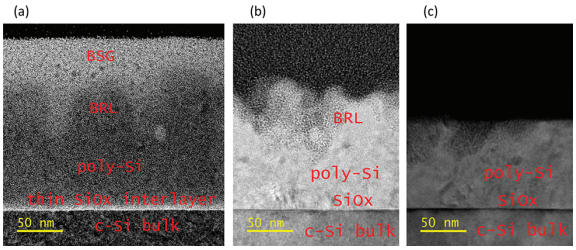

Figure 5. TEM images of the BBr_3-diffused polysilicon contact with different remaining surface layers: (a) BSG/BRL/poly-Si, i.e., the full structure; (b) BRL/poly-Si; and (c) poly-Si. Note that the three images are from different positions of the same wafer, and therefore the small features (e.g., interface shapes) are different.

BSG (a mixture of B_2O_3 and SiO_2) layer is also amorphous, oxygen-rich and silicon-lean. The B-doped poly-Si layer is partially crystallized as well. The level of crystallinity, however, is found to vary across the cm-sized sample wafer, possibly owing to the nonuniform boron diffusion and uneven BSG penetration across the wafer.[23,36] The bulk c-Si region near the SiO_x interface is found to contain a small degree of crystal defects, consistent with previous reports.[37,38]

Unlike $POCl_3$ diffusion, BBr_3 diffusion on silicon is well documented to produce an HF-insoluble Si−B compound (SiB_4 − SiB_6), commonly referred to as a boron-rich layer (BRL), between the BSG and silicon (see refs .21−23 and references therein). The presence of the BRL in our BBr_3-diffused polysilicon samples, between the BSG and the polysilicon layer, is confirmed by the chemical tests (HF immersion and subsequent nitric acid oxidation), as detailed in Experimental Details. However, BRL could not be resolved from the poly-Si layer using HR-TEM, and the small atomic mass of B made it difficult to detect the B distribution using EDS-STEM. The BRL location and thickness in our polysilicon

DOI: 10.1021/acsaem.8b00367
ACS Appl. Energy Mater. 2018, 1, 2275−2282

REC Exhibit 1028, Page 4 of 8

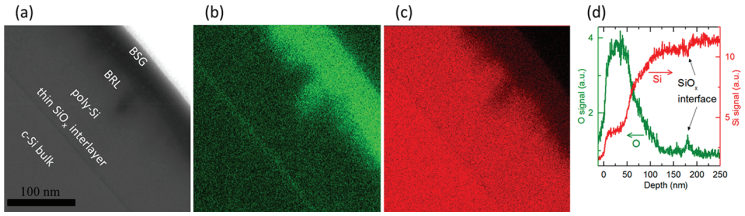

Figure 6. (a) HAADF-STEM image of the BBr_3-diffused polysilicon contact. (b, c) Corresponding EDS-STEM maps of oxygen (O K-map) and silicon (Si K-map), respectively. (d) Line scans across the EDS-STEM maps shown in panels b and c.

samples were hence determined by comparing the TEM images of the samples with different surface layers remaining: BSG/BRL/poly-Si layers, BRL/poly-Si layers, and poly-Si layer alone, as shown in Figure 5.

Furthermore, Figure 5 reveals that the BSG is intertwined with the BRL and the BRL with the poly-Si, such that there is no sharp interface between the different layers. Panels b and c of Figure 5 show that the sample surfaces, which correspond to the BSG/BRL and BRL/poly-Si interfaces respectively, are rather porous. This intermixing phenomenon is particularly strong for the BSG/BRL interface. The intermixed boundaries also contribute to the difficulties in resolving the BRL in this work. Distinction of the BRL from c-Si has been reported in the literature using scanning electron microscopy (SEM), TEM, and EDS.[23,26,39,40] However, in the case of partially amorphous and partially polycrystalline silicon (i.e., the recrystallized poly-Si layer in this study), the amorphous BRL[21] could not be distinguished from the amorphous silicon regions in the poly-Si layer (even from diffraction patterns). Moreover, the different layers are in fact intermixed at the interfaces, making it impossible to separate the individual layers from TEM or EDS-STEM.

The boron-diffused sample also had a high initial bulk Fe_i contamination of 10^{14} cm^{-3}, which was reduced to 3×10^{10} cm^{-3} after forming the polysilicon contacts on both sides. SIMS was used to reveal the surface Fe distribution after contact formation, as shown in Figure 7. A co-processed sample without initial bulk Fe contamination was included as a reference.

As shown in Figure 7, unlike P-doped poly-Si, the B-doped poly-Si layer on its own exhibits a poor gettering effect, which is consistent with the literature regarding the inefficient gettering by heavily B-doped silicon for Fe at thermal diffusion temperatures[26,41] and the weak gettering effects of the undoped poly-Si layer alone.[8]

The Fe-contaminated sample in Figure 7 demonstrates an increase of the Fe concentration in the BRL and at the BSG/BRL interface. As discussed above, the BSG/BRL interface is heavily intermixed, and therefore the layer allocation on the SIMS depth profiles in Figure 7 serves as a rough guide only. The BRL is known to act as a strong gettering site for bulk impurities in silicon,[26,42] whereas the BSG has no gettering effect.[26] Gettering by the BRL can explain the SIMS measurements of higher [Fe] in the BRL and at the intermixed BSG/BRL interface for the sample with initial bulk Fe contamination.

However, the quantitative Fe concentration in the BRL and BSG from the SIMS profile amounts to a bulk Fe concentration of 10^{13} cm^{-3} for a 180-μm thick wafer, which is an order of magnitude lower than the known bulk Fe loss of 10^{14} cm^{-3}. This discrepancy is likely caused by the incorrect calibration

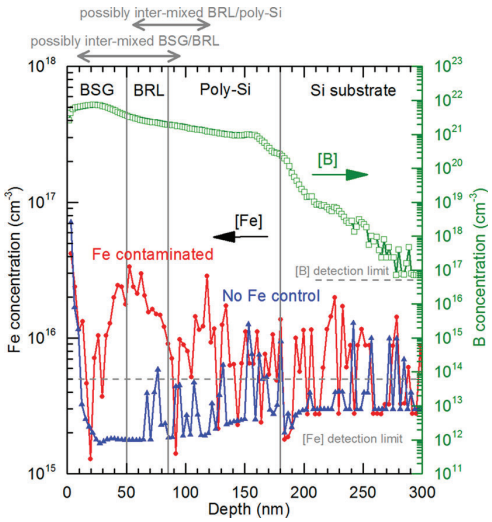

Figure 7. SIMS Fe and B concentrations in BBr_3-diffused polysilicon passivating contact layers and the near-surface silicon substrate, for samples with and without an initial bulk Fe contamination of 10^{14} cm^{-3} prior to the contact formation. Note that the positions of the BSG/BRL and BRL/poly-Si interfaces are indicative only, as the boundaries are intermixed (particularly at the BSG/BRL interface).

standard used in SIMS for quantifying the Fe concentration in the BRL and BSG. The SIMS profiles in Figure 7 are based on the calibrated ion yields of impurities in the silicon matrix. As the BRL (SiB_4–SiB_6)[21,23] and BSG (a mixture of B_2O_3 and SiO_2) are effectively different materials to silicon, the *quantitative* SIMS measurements in the BRL and BSG regions are largely inaccurate. Nevertheless, the qualitative comparison of the SIMS Fe profiles for the two samples with and without initial bulk Fe contamination is still a sufficient proof of the gettering effect of the BRL.

To further confirm that bulk Fe is gettered to the BRL, a post-diffusion oxidation at a high temperature (930 °C) was carried out on samples with different surface layers, as shown in Figure 8. Two of the samples were oxidized with the BRL remaining in place, in either the BSG/BRL/poly-Si structure or the BRL/poly-Si structure. The other sample had the BRL chemically removed prior to the high-temperature oxidation and was oxidized with only the poly-Si layer remaining.

The BRL is known to be easily oxidized into the BSG during a post-diffusion oxidation.[23] At moderate and high temperatures where Fe is sufficiently mobile, oxidation of the BRL into BSG is found to drive the previously gettered impurities back into the silicon wafer bulk.[26] The boiling nitric acid oxidation (~100 °C), which was used to chemically remove the BRL, is unable to cause any measurable Fe diffusion into silicon. The

DOI: 10.1021/acsaem.8b00367
ACS Appl. Energy Mater. 2018, 1, 2275−2282

REC Exhibit 1028, Page 5 of 8

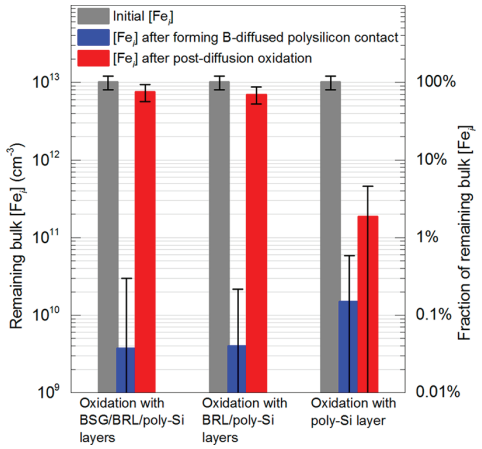

Figure 8. Fe_i concentrations in the silicon wafer bulk at three different stages: before processing, after forming BBr_3 diffusion-doped polysilicon contacts (slightly different gettering effects that arose from different diffusion temperatures), and after further post-diffusion oxidation with different surface layers being present.

results presented in Figure 8 demonstrate that when the BRL is present during the high-temperature oxidation, regardless of the presence of the BSG, most of the initially gettered Fe reappears in the silicon wafer bulk. On the other hand, for the sample undergoing a high-temperature oxidation without the BRL, the bulk Fe concentration remains low. These results therefore confirm that the BRL is the main gettering site in boron diffusion-doped polysilicon passivating contacts. Similar to phosphorus-doped polysilicon, the gettering of Fe by the BRL is also driven by an impurity segregation mechanism. However, the underlying physics for the higher impurity solubility in the BRL has not yet been studied.

4. DISCUSSION

Results in this work clearly show that two different materials are responsible for the gettering effects of phosphorus and boron diffusion-doped polysilicon passivating contacts: in the case of phosphorus, the heavily phosphorus-doped polysilicon acts as the gettering site; and in the case of boron, the boron-rich layer (i.e., the HF-insoluble Si−B compound) accounts for the strong gettering effects. This paves the way for further detailed investigation of the underlying atomic-scale gettering reactions. The findings also explain why certain polysilicon passivating contacts exhibit effective gettering while others do not[8,9] and has implications for the polysilicon doping techniques.

The finding that impurities are gettered by the heavily P-doped polysilicon explains the reported bulk carrier lifetime improvements after the formation of phosphorus ion-implanted polysilicon passivating contacts.[9] Given a sufficient thermal budget for bulk impurities to reach the wafer surfaces and travel through the thin oxide interlayers, other techniques that heavily dope the polysilicon layers by phosphorus atoms, for example via an in situ doping and subsequent annealing, are also likely to generate impurity gettering effects.

Boron-doped polysilicon passivating contacts from ion implantation and annealing, on the other hand, have been reported to have no gettering effect.[9] This is consistent with our finding that the BRL, from BBr_3 thermal diffusion on polysilicon, is responsible for the gettering effect in boron diffusion-doped polysilicon contacts. Boron doping via spin-on, printed, or chemical vapor deposited surface dopant sources, followed by a drive-in anneal, has also been reported to produce the BRL in silicon surface regions.[39,40,43] These techniques, as well as others that cause a significant boron "pile-up" to create the BRL, could potentially be used for doping the polysilicon contacts in order to accomplish both contact formation and impurity gettering effects.

In boron-diffused crystalline silicon, the BRL has to be removed, commonly via a post-diffusion oxidation, to allow adequate passivation of the boron-doped c-Si surfaces, which unfortunately repoisons the silicon wafer bulk.[26] As the presence of the BRL and its gettered impurities are found to have no impact on the excellent surface passivation of the polysilicon contacts,[8] and they do not impair the formation of a metal contact, boron diffusion-doped polysilicon passivating contacts demonstrate obvious dual benefits compared to the conventional boron diffusion doping on c-Si wafers.

As the surface layers (phosphorus-doped polysilicon or boron-rich layers) are found to be the gettering sites in polysilicon passivating contacts, the strong gettering effects of these contacts partially benefit from the high-temperature processes used for the contact formation, which provide the necessary thermal budgets for the impurity migration toward the surface gettering layers. To achieve similar impurity gettering effects, for example via a conventional phosphorus diffusion, low-temperature processed passivating contacts, such as the amorphous silicon based heterojunction silicon solar cells, would require an additional pretreatment at sufficiently high gettering temperatures.

5. CONCLUSION

In summary, this work presents a direct observation of the impurity redistribution during the formation of both phosphorus and boron diffusion-doped polysilicon passivating contacts. This allows for a conclusive identification of the two very different gettering sites in phosphorus- and boron-diffused contacts: for phosphorus-doped polysilicon contacts, impurities are found to be gettered from the silicon wafer bulk to the heavily phosphorus-doped polysilicon layer; whereas for the boron-doped polysilicon contacts, the presence of a boron-rich layer (a Si−B compound, SiB_4− SiB_6), from thermal diffusion for example, is the key to achieving strong gettering effects for the bulk impurities. These findings provide an improved understanding of the impurity gettering mechanisms in polysilicon-based passivating contact structures, and locating the respective gettering sites is the first step toward an in-depth understanding of the atomic-scale interactions of impurities with the gettering agents.

■ AUTHOR INFORMATION

Corresponding Author

*E-mail: anyao.liu@anu.edu.au.

ORCID

AnYao Liu: 0000-0003-4579-5495

Sieu Pheng Phang: 0000-0002-5664-8012

Notes

The authors declare no competing financial interest.

■ ACKNOWLEDGMENTS

This work has been supported by the Australian Renewable Energy Agency (ARENA) through Project RND009. A.Y.L. is supported by the Australian Centre for Advanced Photovoltaics

DOI: 10.1021/acsaem.8b00367
ACS Appl. Energy Mater. 2018, 1, 2275−2282

REC Exhibit 1028, Page 6 of 8

(ACAP) Postdoctoral Fellowship. We acknowledge access to NCRIS facilities, the Australian National Fabrication Facility (ANFF) ACT node, the Heavy Ion Accelerator Capability, and the Australian Microscopy & Microanalysis Research Facility at the Centre of Advanced Microscopy, at the Australian National University.

■ REFERENCES

(1) Yoshikawa, K.; Kawasaki, H.; Yoshida, W.; Irie, T.; Konishi, K.; Nakano, K.; Uto, T.; Adachi, D.; Kanematsu, M.; Uzu, H.; Yamamoto, K. Silicon Heterojunction Solar Cell with Interdigitated Back Contacts for a Photoconversion Efficiency over 26%. *Nat. Energy* **2017**, *2*, 17032.

(2) Richter, A.; Benick, J.; Feldmann, F.; Fell, A.; Hermle, M.; Glunz, S. W. N-Type Si Solar Cells with Passivating Electron Contact: Identifying Sources for Efficiency Limitations by Wafer Thickness and Resistivity Variation. *Sol. Energy Mater. Sol. Cells* **2017**, *173*, 96−105.

(3) Haase, F.; Kiefer, F.; Schäfer, S.; Kruse, C.; Krügener, J.; Brendel, R.; Peibst, R. Interdigitated Back Contact Solar Cells with Polycrystalline Silicon on Oxide Passivating Contacts for Both Polarities. *Jpn. J. Appl. Phys.* **2017**, *56*, 08MB15.

(4) Zhao, J.; Wang, A.; Green, M. A. 24.5% Efficiency Silicon PERT Cells on MCZ. Substrates and 24.7% Efficiency PERL Cells on FZ. Substrates. *Prog. Photovoltaics* **1999**, *7*, 471−474.

(5) Benick, J.; Richter, A.; Müller, R.; Hauser, H.; Feldmann, F.; Krenckel, P.; Riepe, S.; Schindler, F.; Schubert, M. C.; Hermle, M.; Bett, A. W.; Glunz, S. W. High-Efficiency N-Type HP mc Silicon Solar Cells. *IEEE J. Photovolt.* **2017**, *7*, 1171−1175.

(6) Post, I. R. C.; Ashburn, P.; Wolstenholme, G. R. Polysilicon Emitters for Bipolar Transistors: a Review and Re-evaluation of Theory and Experiment. *IEEE Trans. Electron Devices* **1992**, *39*, 1717−1731.

(7) Patton, G. L.; Bravman, J. C.; Plummer, J. D. Physics, Technology, and Modeling of Polysilicon Emitter Contacts for VLSI Bipolar Transistors. *IEEE Trans. Electron Devices* **1986**, *33*, 1754−1768.

(8) Liu, A. Y.; Yan, D.; Phang, S. P.; Cuevas, A.; Macdonald, D. Effective Impurity Gettering by Phosphorus- and Boron-diffused Polysilicon Passivating Contacts for Silicon Solar Cells. *Sol. Energy Mater. Sol. Cells* **2018**, *179*, 136−141.

(9) Krügener, J.; Haase, F.; Rienäcker, M.; Brendel, R.; Osten, H. J.; Peibst, R. Improvement of the SRH Bulk Lifetime upon Formation of N-type POLO Junctions for 25% Efficient Si Solar Cells. *Sol. Energy Mater. Sol. Cells* **2017**, *173*, 85−91.

(10) Zoth, G.; Bergholz, W. A Fast, Preparation-free Method to Detect Iron in Silicon. *J. Appl. Phys.* **1990**, *67*, 6764−6771.

(11) Macdonald, D. H.; Geerligs, L. J.; Azzizi, A. Iron Detection in Crystalline Silicon by Carrier Lifetime Measurements for Arbitrary Injection and Doping. *J. Appl. Phys.* **2004**, *95*, 1021−1028.

(12) Yan, D.; Cuevas, A.; Bullock, J.; Wan, Y.; Samundsett, C. Phosphorus-diffused Polysilicon Contacts for Solar Cells. *Sol. Energy Mater. Sol. Cells* **2015**, *142*, 75−82.

(13) Yan, D.; Cuevas, A.; Wan, Y.; Bullock, J. Passivating Contacts for Silicon Solar Cells Based on Boron-diffused Recrystallized Amorphous Silicon and Thin Dielectric Interlayers. *Sol. Energy Mater. Sol. Cells* **2016**, *152*, 73−79.

(14) Liu, A. Y.; Sun, C.; Markevich, V. P.; Peaker, A. R.; Murphy, J. D.; Macdonald, D. Gettering of Interstitial Iron in Silicon by Plasma-enhanced Chemical Vapour Deposited Silicon Nitride Films. *J. Appl. Phys.* **2016**, *120*, 193103.

(15) Liu, A. Y.; Macdonald, D. Impurity Gettering Effect of Atomic Layer Deposited Aluminium Oxide Films on Silicon Wafers. *Appl. Phys. Lett.* **2017**, *110*, 191604.

(16) Liu, A. Y.; Macdonald, D. Impurity Gettering by Atomic-Layer-Deposited Aluminium Oxide Films on Silicon at Contact Firing Temperatures. *Phys. Status Solidi RRL* **2018**, *12*, 1700430.

(17) Istratov, A. A.; Hieslmair, H.; Weber, E. R. Iron and its Complexes in Silicon. *Appl. Phys. A: Mater. Sci. Process.* **1999**, *69*, 13−44.

(18) Sinton, R. A.; Cuevas, A. Contactless Determination of Current-voltage Characteristics and Minority-carrier Lifetimes in Semiconductors from Quasi-steady-state Photoconductance Data. *Appl. Phys. Lett.* **1996**, *69*, 2510−2512.

(19) Geerligs, L.; Macdonald, D. Dynamics of Light-induced FeB pair Dissociation in Crystalline Silicon. *Appl. Phys. Lett.* **2004**, *85*, 5227−5229.

(20) Mayer, J.; Giannuzzi, L. A.; Kamino, T.; Michael, J. TEM Sample Preparation and FIB-induced Damage. *MRS Bull.* **2007**, *32*, 400−407.

(21) Arai, E.; Nakamura, H.; Terunuma, Y. Interface Reactions of B2O3-Si System and Boron Diffusion into Silicon. *J. Electrochem. Soc.* **1973**, *120*, 980−987.

(22) Negrini, P.; Ravaglia, A.; Solmi, S. Boron Predeposition in Silicon Using BBr3. *J. Electrochem. Soc.* **1978**, *125*, 609−613.

(23) Kessler, M. A.; Ohrdes, T.; Wolpensinger, B.; Harder, N.-P. Charge Carrier Lifetime Degradation in Cz Silicon through the Formation of a Boron-rich Layer during BBr3 Diffusion Processes. *Semicond. Sci. Technol.* **2010**, *25*, 055001.

(24) Busen, K.; FitzGibbons, W.; Tsang, W. Ellipsometric Investigations of Boron-Rich Layers on Silicon. *J. Electrochem. Soc.* **1968**, *115*, 291−294.

(25) Kobayashi Asuha, H.; Maida, O.; Takahashi, M.; Iwasa, H. Nitric Acid Oxidation of Si to Form Ultrathin Silicon Dioxide Layers with a Low Leakage Current Density. *J. Appl. Phys.* **2003**, *94*, 7328−7335.

(26) Phang, S. P.; Liang, W.; Wolpensinger, B.; Kessler, M. A.; Macdonald, D. Tradeoffs Between Impurity Gettering, Bulk Degradation, and Surface Passivation of Boron-Rich Layers on Silicon Solar Cells. *IEEE J. Photovolt.* **2013**, *3*, 261−266.

(27) Wagner, H.; Dastgheib-Shirazi, A.; Min, B.; Morishige, A. E.; Steyer, M.; Hahn, G.; del Cañizo, C.; Buonassisi, T.; Altermatt, P. P. Optimizing Phosphorus Diffusion for Photovoltaic Applications: Peak Doping, Inactive Phosphorus, Gettering, and Contact Formation. *J. Appl. Phys.* **2016**, *119*, 185704.

(28) Vähänissi, V.; Haarahiltunen, A.; Talvitie, H.; Yli-Koski, M.; Savin, H. Impact of Phosphorus Gettering Parameters and Initial Iron Level on Silicon Solar Cell Properties. *Prog. Photovoltaics* **2013**, *21*, 1127−1135.

(29) Schön, J.; Vähänissi, V.; Haarahiltunen, A.; Schubert, M. C.; Warta, W.; Savin, H. Main Defect Reactions behind Phosphorus Diffusion Gettering of Iron. *J. Appl. Phys.* **2014**, *116*, 244503.

(30) Carabelas, A.; Nobili, D.; Solmi, S. Grain Boundary Segregation in Silicon Heavily Doped with Phosphorus and Arsenic. *J. Phys. Colloques* **1982**, *43*, C1-187−C1−192.

(31) Rose, J. H.; Gronsky, R. Scanning Transmission Electron Microscope Microanalytical Study of Phosphorus Segregation at Grain Boundaries in Thin-film Silicon. *Appl. Phys. Lett.* **1982**, *41*, 993−995.

(32) Broniatowski, A. Electrical Measurement of the Dopant Segregation Profile at the Grain Boundary in Silicon Bicrystals. *J. Appl. Phys.* **1988**, *64*, 4516−4525.

(33) Murphy, J. D.; Falster, R. J. Contamination of Silicon by Iron at Temperatures Below 800 °C. *Phys. Status Solidi RRL* **2011**, *5*, 370−372.

(34) Myers, S. M.; Seibt, M.; Schröter, W. Mechanisms of Transition-metal Gettering in Silicon. *J. Appl. Phys.* **2000**, *88*, 3795−3819.

(35) Solmi, S.; Parisini, A.; Angelucci, R.; Armigliato, A.; Nobili, D.; Moro, L. Dopant and Carrier Concentration in Si in Equilibrium with Monoclinic SiP Precipitates. *Phys. Rev. B: Condens. Matter Mater. Phys.* **1996**, *53*, 7836−7841.

(36) Wada, Y.; Nishimatsu, S. Grain Growth Mechanism of Heavily Phosphorus-Implanted Polycrystalline Silicon. *J. Electrochem. Soc.* **1978**, *125*, 1499−1504.

(37) Snel, J. The Doped Si/SiO2 Interface. *Solid-State Electron.* **1981**, *24*, 135−139.

DOI: 10.1021/acsaem.8b00367
ACS Appl. Energy Mater. 2018, 1, 2275−2282

REC Exhibit 1028, Page 7 of 8

(38) Cousins, P. J.; Cotter, J. E. The Influence of Diffusion-induced Dislocations on High Efficiency Silicon Solar Cells. *IEEE Trans. Electron Devices* **2006**, *53*, 457−464.
(39) Mok, K. C.; Van De Loo, B. W.; Vlooswijk, A. H.; Kessels, W. E.; Nanver, L. K. Boron-Doped Silicon Surfaces From B2H6 Passivated by ALD Al2O3 for Solar Cells. *IEEE J. Photovolt.* **2015**, *5*, 1310−1318.
(40) Ryu, K.; Upadhyaya, A.; Song, H.-J.; Choi, C.-J.; Rohatgi, A.; Ok, Y.-W. Chemical Etching of Boron-rich Layer and its Impact on High Efficiency N-type Silicon Solar Cells. *Appl. Phys. Lett.* **2012**, *101*, 073902.
(41) McHugo, S. A.; McDonald, R. J.; Smith, A. R.; Hurley, D. L.; Weber, E. R. Iron Solubility in Highly Boron-doped Silicon. *Appl. Phys. Lett.* **1998**, *73*, 1424−1426.
(42) Libal, J.; Petres, R.; Buck, T.; Kopecek, R.; Hahn, G.; Ferre, R.; Vetter, M.; Martin, I.; Wambach, K.; Fath, P. N-type Multicrystalline Silicon Solar Cells: BBr3-diffusion and Passivation of p+-diffused Silicon Surfaces. *Proceedings of the 20th European Photovoltaic Solar Energy Conference*; WIP Renewable Energies: Munich, Germany, 2005; pp 793−796.
(43) Singha, B.; Solanki, C. S. Impact of a Boron Rich Layer on Minority Carrier Lifetime Degradation in Boron Spin-on Dopant Diffused N-type Crystalline Silicon Solar Cells. *Semicond. Sci. Technol.* **2016**, *31*, 035009.

DOI: 10.1021/acsaem.8b00367
ACS Appl. Energy Mater. 2018, 1, 2275−2282

REC Exhibit 1028, Page 8 of 8